Enzymatic reduction of oxygen by small laccase. A rapid freeze-quench EPR study

Nami, F.

Chapter 1

Introduction

This chapter provides a general introduction about the enzyme and the techniques used in this thesis. The outline of the thesis is also presented.

1.1 Motivation

Aerobic organisms including humans utilize molecular oxygen as a final electron acceptor to harness the energy provided by the oxygen-to-water conversion. While O_2 is essential for their life, it can also be harmful if partially reduced, resulting in the production of reactive oxygen species (ROS). To effectively utilize O_2, the organism employs metal-containing enzymes to assist in the reduction of O_2 to H_2O without releasing ROS. The two enzymatic systems that have the capability to catalyze this process are the multicopper oxidases (MCO's) and cytochrome *c* oxidase (C*c*O)[1]. The function of C*c*O, the terminal enzyme in the respiration chain, is based on using copper and iron ions[2] while MCO's utilize exclusively copper ions to catalyze the process. In this thesis, we focus on understanding the mechanism of O_2 reduction by an MCO, the small laccase (SLAC) from *Streptomyces coelicolor,* using multi-frequency electron paramagnetic resonance (EPR) spectroscopy in combination with the rapid freeze-quench (RFQ) technique.

1.2 Multicopper oxidases

The MCO's couple the four single-electron oxidations of a substrate to the four-electron reduction of oxygen[3]. Based on their substrates, MCO's play different roles in various organisms. For instance, ceruloplasmin is a ferroxidase that catalyzes the conversion of Fe (II) to Fe(III) in mammalian cells[4] and CueO is a copper oxidase that catalyzes the conversion of Cu (I) to Cu(II) in *E. Coli*[5]. Laccases play a variety of roles in bacteria, plants and fungi including the formation / degradation of lignin and the biosynthesis of antibiotics, as they can oxidize a wide range of aromatic compounds[6,7].

Structurally, MCO's contain at least four copper ions, which are distributed in three sites, a type 1 (T1 Cu), a type 2 (T2 Cu) and a type 3 (T3 Cu) site[8], as represented for SLAC in figure1.1[9]. The T1 Cu, called blue copper, is

coordinated by two histidines (His) and one cysteine (Cys), while the fourth ligand varies among proteins. The so-called charge-transfer transition from S(Cys) to Cu(II) results in an intense absorption band around 600 nm giving rise to the blue color of T1 Cu-containing proteins[10]. The T2 Cu is commonly coordinated by two His's and a water or hydroxide ion and shows no appreciable absorption in the visible. The two T3 Cu's form a binuclear copper center. In the resting form of the enzyme, the copper ions are bridged by a hydroxide ion. Each T3 Cu is coordinated to three His's and characterized by an absorption shoulder at about 330nm. The T2 Cu and the two T3 Cu's form a trinuclear cluster (TNC). The T1 Cu, at a distance of about 13 Å from the TNC, is the primary electron acceptor from the substrate. The electrons are subsequently transferred through the Cys-His pathway to the TNC, where O_2 binds and gets reduced. For an introduction to the mechanism of oxygen reduction at the TNC we refer to chapter 6.

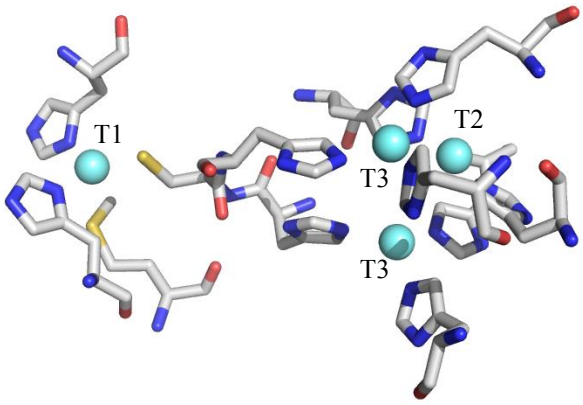

Figure 1.1. The active site of small laccase from *S. coelicolor* (PDB: 3CG8). The coordinated residues are represented by sticks. Color code: Cu, cyan; C, gray; N, blue; O, red; S, yellow.

1.3 Small laccase

During 2004 a new MCO called SLAC has been identified when searching the genome of *S. coelicolor* for the presence of copper proteins[11]. Analysis of the SLAC sequence revealed that the enzyme consists of 343 amino acids. The molecular weight was estimated to be 36.9 kDa, smaller than the 60-70 kDa of common laccases. The 3D structure of the protein revealed that SLAC represents structural features distinct from those of other MCO's[9]. The SLAC enzyme consists of only two cupredoxin-like domains and it is active as a homotrimer, contrary to the more common three-domain MCO's (3dMCO) such as three-domain laccases (3dLACs), ascorbate oxidase, CueO and Fet3p, which are active in monomeric form[8] (figure 1.2). However, the active-site morphology of SLAC, which involves the T1 Cu and the TNC, is the same as for other MCO's. In SLAC, the TNC is located at the interface of the two monomers, while in 3dMCO's the TNC is located between domain 1 and 3[9].

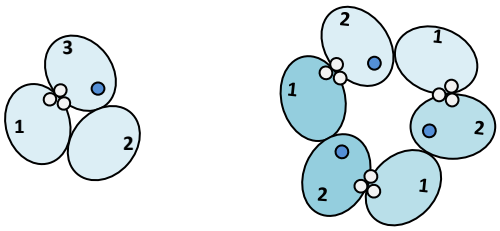

Figure 1.2. Cartoon representation of the domain organization and the copper sites for a 3dMCO (left) and for SLAC (right). Different monomers are characterized by the level of blue color. The T1 Cu's are shown as small blue circles and the TNC's as triplets of gray circles.

In our mechanistic study of the reduction of oxygen by SLAC, we have used the wild-type enzyme and several mutants. In the mutants, the T1 Cu-coordinating cysteine was replaced by serine. Spectroscopic and biochemical characterization

reveals that this mutation results in an empty T1 site while the TNC is intact[12]. Surprisingly, the type 1 copper depleted (T1D) SLAC is still able to complete the reduction of O_2 to H_2O[12], while for 3dMCO's in the absence of T1 Cu the reduction of O_2 stops at the peroxide level. Reaction of the reduced T1D SLAC with oxygen results in the formation of a biradical intermediate detected by EPR on the time scale of minutes[12]. For many enzymatic systems, it has been reported that the radical intermediate trapped on the time scale of seconds/minutes differs from the initially generated radical[13]. The initial radical, which is mechanistically more interesting, can migrate to a more stable location. Therefore, it is important to trap intermediates on the sub-seconds time scale in order to be able to characterize the mechanistically important species by EPR. To that end, in chapters 4 and 5, we employ the rapid freeze-quench technique to study the intermediates in the reoxidation of reduced T1D SLAC and reduced wt SLAC on the time scale of milliseconds.

1.4 Rapid freeze-quench

Rapid freeze-quench, being introduced in 1961[14], is a proven technique to trap the intermediates in a biochemical reaction on the time scale of milliseconds. In RFQ, the reaction components are rapidly mixed and after a certain reaction time the reaction mixture is suddenly frozen in a cryomedium. Then the frozen particles are collected from the cryomedium and subjected to different spectroscopic techniques.

A schematic drawing of the RFQ apparatus used in our research is shown in figure 1.3. The syringe ram (C) is used to push fluid from a syringe under predetermined conditions and the desired parameters such as ram velocity and the displacement of each push are set by the ram controller (A). Before loading the reagents, the syringes (D) are assembled and mounted on top of the syringe ram. Loading the reagents can be done by manual displacement of the ram or by

using the ram controller. The use of a manual loading provides better control over the speed and consequently reduces the chance of drawing in air. Both syringes are generally filled simultaneously. When the syringes are filled with the reagents, any air bubbles in the syringes and coupling hose are carefully expelled by moving the ram forward. Remaining air bubbles lead to a substantial deceleration of the flow when the solutions are injected, resulting in the formation of droplets with unknown reaction time. Air bubbles also cause dribbling of the reacted solution from the outlet nozzle leading to relatively big frozen particles.

The mixer (F) is connected to the sample syringes via the coupling hoses (E) in a T-shaped inlet arrangement. The mixing starts when the two reagents meet and is complete before the reaction mixture reaches the aging hose.

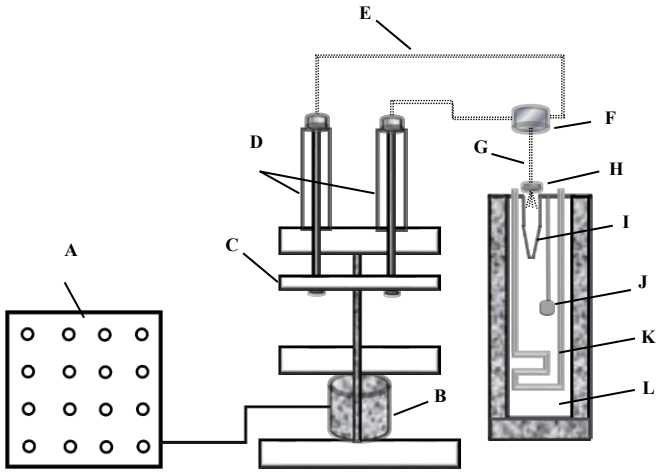

Figure 1.3. Schematic drawing of the rapid freeze-quench apparatus. A: ram controller, B: DC servo motor, C: ram, D: syringes, E: coupling hoses, F: mixer, G: aging hose, H: nozzle, I: glass tube, J: stirrer, K: low-temperature nitrogen stream, L: isopentane bath.

The reaction takes place in the aging hose (G), which connects the outlet of the mixer to the spray nozzle (H). Isopentane is the most common solvent in rapid

freezing as it is liquid at room temperature and freezes only at 113 K. Isopentane is used as the bath and freezing solvent at the typical temperature of –130 to –140 °C. The isopentane bath (L) is continuously stirred (J) to ensure a homogeneous temperature. Once the isopentane in the tube (I) reaches the desired temperature, the sample preparation starts. The reagents are rapidly mixed and the reaction mixture is sprayed through the nozzle into the cold isopentane, which causes instantaneous quenching of the reaction.

In our research, we have combined the RFQ technique with EPR in the study of SLAC. A serious difficulty, which has limited the application of the RFQ technique in the study of enzymatic reactions, is collecting the small freeze-quench particles from isopentane into an EPR tube[15]. As a consequence of the inefficiency of the packing procedure, a large amount of sample is required. This might be prohibitive in particular for proteins, for which often limited amounts are available. In chapter 2, a new method is reported, which we have developed to improve the collection of freeze-quench particles from isopentane and their packing into an EPR tube with an inner diameter of 3 mm for the conventional 9 GHz (X-band) experiments[16]. The method is based on sucking the particle suspension into an EPR tube with a filter at the bottom. Isopentane exits through the filter and the frozen particles remain in the tube. This development results in a significant reduction of the required volume of reactants by a more quantitative collection of the frozen particles, from which we benefitted in the studies on SLAC.

As yet, the RFQ technique was mostly combined with EPR spectroscopy at X-band. Mechanistic studies would benefit significantly from an extension to other microwave frequencies. However, scaling up of RFQ/EPR to higher microwave frequencies is not trivial. While EPR tubes with an inner diameter of 3 mm are being used at X-band, single-mode cavities at higher microwave frequencies

can only accommodate capillaries with sub-millimeter diameters. In chapter 3, we demonstrate a systematic approach to the combination of the rapid-freeze-quench technique with EPR spectroscopy at microwave frequencies up to 275 GHz. The method described in chapter 2 has been extended to capillaries with an inner diameter of only 150 μm. In chapters 4 and 5, we make use of this approach to RFQ in the preparation of samples of SLAC for EPR experiments at 9, 94 and 275 GHz.

1.5 EPR spectroscopy

The main spectroscopic technique used in the research reported in this thesis is Electron Paramagnetic Resonance (EPR) spectroscopy. In EPR spectroscopy, transitions between spin sublevels of a paramagnetic center in an external magnetic field are induced by microwave radiation. In the resting form of SLAC, the copper ions are in the oxidized state, Cu(II). The electron configuration of Cu(II) is $(3d)^9$, which results in a net spin S=1/2. Both the T1 Cu(II) and the T2 Cu(II) are EPR active, while the T3 Cu (II)'s are EPR silent due to their antiferromagnetic coupling. The T1 and T2 Cu's show distinct EPR spectra, as the coordinated ligands are different. The ligands affect the wavefunction of the 3d electrons of copper through covalent bonds and electrostatic interactions[16].

To describe the EPR spectrum of a Cu(II) ion, at least two terms should be considered in the spin Hamiltonian.

$$H = \beta_e \vec{B} \cdot \vec{\vec{g}} \cdot \vec{S} + \vec{S} \cdot \vec{\vec{A}} \cdot \vec{I}$$

The first term represents the interaction of the electron spin with the external magnetic field, the electron Zeeman interaction, where β_e is the Bohr magneton,

$\vec{B}$ is the external magnetic field, $\vec{\vec{g}}$ is the *g*-tensor and $\vec{S}$ is the electron spin angular momentum operator. The anisotropic deviation from the value of g = 2.0023 for a free electron due to spin-orbit coupling is described by the g-tensor. The second term represents the hyperfine interaction of the electron spin with the nuclear spin of copper (I=3/2), where $\vec{\vec{A}}$ is the hyperfine tensor and $\vec{I}$ is the nuclear spin angular momentum operator. The hyperfine interaction results in the splitting of each electron-spin transition into (2I + 1) lines, which means four lines for copper.

The EPR spectrum of Cu(II) is described by the principal values g_x, g_y, and g_z of the *g* tensor (with $g_z > g_y > g_x$) and the principal values A_x, A_y, and A_z of the *A* tensor of copper. We assume the principal axes of both tensors to be parallel. Figure 1.4 shows simulated EPR spectra for typical T1 Cu and T2 Cu centers in frozen solution at two different microwave frequencies, at 9.5 and at 275 GHz. At 9.5 GHz, the g_x and g_y transition around 330 mT are not resolved. The g_z transition at lower magnetic field in both cases shows the copper-hyperfine splitting, which is significantly larger for T2 Cu than for T1 Cu. At 275 GHz, the *g*-resolution is complete at the cost of the hyperfine resolution. The g_x and g_y transitions are nicely resolved between 9.4 and 9.7 T for T1 Cu and for T2 Cu, while the field-independent hyperfine splitting determines the line width of the g_z transition but is not resolved.

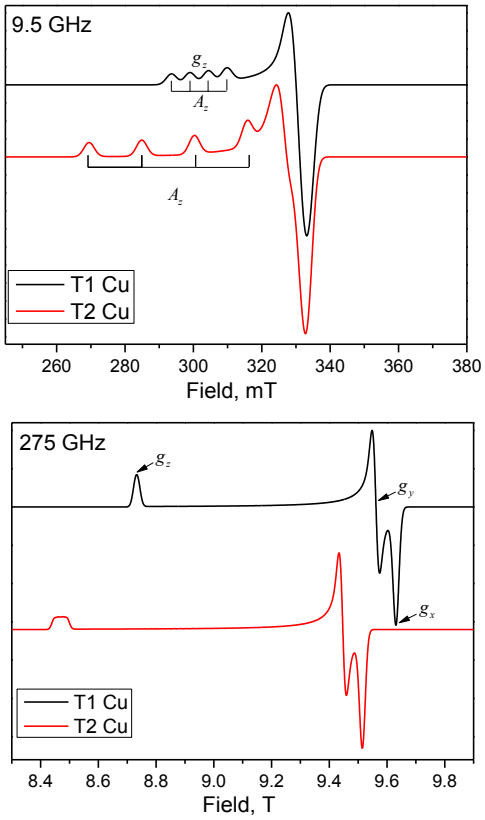

Figure 1.4. Typical simulated EPR spectra of T1 Cu and T2 Cu at two microwave frequencies of 9.5 and 275 GHz. The spectra are simulated with EasySpin[17] for frozen solutions at 40 K using the g-values of (2.040, 2.055, 2.25) and A-values of (35 40 170) in MHz for T1 Cu and the g-values of (2.065, 2.080, 2.32) and A-values of (35 40 500) in MHz for T2 Cu.

In figure 1.5, EPR spectra of T1D SLAC at 9.5 and 275 GHz are presented. Comparison of the T1D SLAC spectrum at 9.5 GHz with the model simulations in figure 3 shows that the spectrum at 9.5 GHz has the overall structure that we expect for T2 Cu, and at the same time that EPR spectra for copper sites in proteins will in general be more complicated than for model centers. The lines at 272, at 293, and at 314 mT indicate a hyperfine interaction characteristic for

T2 Cu, with the fourth hyperfine line hidden in the g_x, g_y region. In addition to the copper hyperfine structure, the spectrum nicely shows a small but resolved hyperfine structure around 328 mT, which derives from the interaction of the electron spin with the nitrogen nuclei of the copper-coordinating histidines. Additional lines at 282 and 305 mT point to the contribution of a second, distinct copper site. At 275 GHz, the higher *g*-resolution clearly reveals the two copper sites with g_z transitions at 8.37 and 8.77 T, while the corresponding g_x and g_y transitions are still not completely resolved. As expected, the copper hyperfine splitting is not resolved at this high microwave frequency. The combination of the experimental data at 9.5 and 275 GHz allows the simulation of the EPR spectra. The result is shown in figure 1.5, where we have not taken into account the nitrogen hyperfine interaction in the simulation. From the simulation we obtain the spin Hamiltonian parameters for the two Cu's (values in legend of figure 1.5), which have the same g_x and different g_y, g_z, and A_z. Apparently, the T2 Cu site of T1D SLAC consists of two populations, in which the copper may have a different ligand besides the coordinating histidines. The difference that remains between the experimental spectrum and the simulated spectrum at 275 GHz around 9.52 T (figure 1.5) indicates a small contribution of a third copper species. The small signals around 9.85 T in the experimental spectrum at 275 GHz arise from a Mn(II) impurity in the sample.

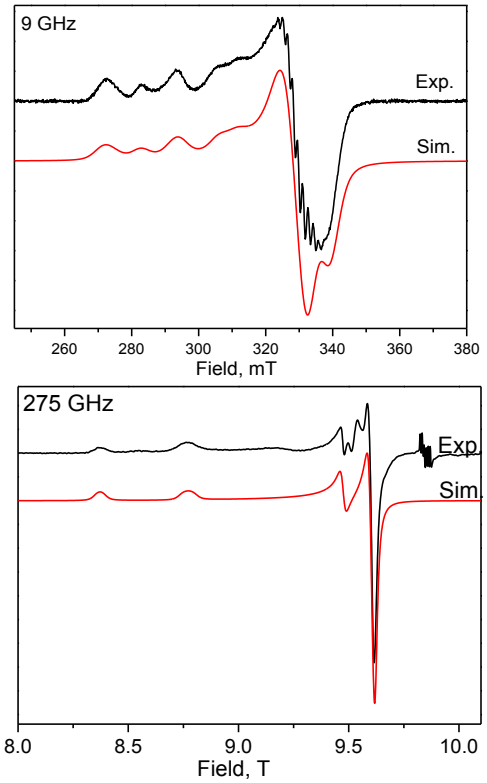

Figure 1.5. Experimental and simulated EPR spectra of the resting form of T1D SLAC (as purified) at two microwave frequencies of 9.5 and 275 GHz. The small signals around 9.85 T in the experimental spectrum at 275 GHz arise from a Mn(II) impurity in the sample. Enzyme concentration is 400 μM and 3mM, for the measurement at 9.5 and 275.7 GHz, respectively, both in 100 mM sodium phosphate buffer, pH 6.8. EPR measurements at 9.5 GHz, T = 40 K, microwave power 0.16 mW and modulation amplitude 0.5 mT. EPR measurements at 275.7 GHz, T = 10 K, microwave power 100 nW and modulation amplitude 2.4 mT. The spectra are simulated with EasySpin[17] for frozen solutions at the same temperature as for the experimental spectra using the g-values of (2.048, 2.052, 2.25) and A-values of (35 30 590) in MHz for one component and the g-values of (2.048, 2.079, 2.35) and A-values of (35 30 380) in MHz for the second component. A g-strain of (0.0015 0.0025 0.0080) is included for both components.

In order to understand the EPR spectra of the biradical intermediate formed during the reoxidation of T1D SLAC, which is part of chapter 4, we consider a system of two interacting spins $s_1 = s_2 = 1/2$. Besides the interaction with the external magnetic field, the spins are subject to dipolar and exchange interaction. To get a feeling for the type of EPR spectra one can get, we, for the moment, neglect the dipolar interaction and consider the following spin Hamiltonian.

$$H = \beta_e B \left(g_1 s_{1z} + g_2 s_{2z} \right) - J\vec{s}_1 \cdot \vec{s}_2$$

where the magnetic field is taken in the z-direction, the two spins have isotropic *g*-values g_1 and g_2, and *J* represents the exchange interaction. We describe the energy-level scheme and the corresponding EPR transitions for two limiting cases, for weak and strong coupling of the spins[18].

Weak coupling: $|J| \ll (|g_1 - g_2|)\beta_e B$

In this case we start from the eigenfunctions $|m_{s1}\ m_{s2}\rangle$ of the Zeeman part of the spin Hamiltonian: $|½\ ½\rangle$, $|½\ -½\rangle$, $|-½\ ½\rangle$, $|-½\ -½\rangle$. The corresponding energy eigenvalues are given in the energy-level scheme in figure 1.6a, left. Upon introduction of a small exchange coupling, the energies of the spin states increase/decrease by 1/4 *J*, as is clear from the exchange term in the spin Hamiltonian. This is shown in figure 1.6a, right, where also the EPR transitions are represented according to the selection rule $\Delta m_s = \pm 1$ for either one or the other electron spin. The EPR spectrum corresponds to a pair of doublet transitions, centered at the resonance fields for spin 1 and spin 2, respectively, with doublet splitting determined by the exchange interaction.

Strong coupling: $|J| \gg (|g_1 - g_2|)\beta_e B$

In this case we start from the eigenfunctions $|S\ M_S\rangle$ of the exchange part of the spin Hamiltonian: $|1\ 1\rangle$,

$|1\ 0\rangle$, $|1\ -1\rangle$, $|0\ 0\rangle$, which represent the three triplet states and one singlet state of the coupled S=1 system. The corresponding energy eigenvalues are given in the energy level scheme in figure 1.6b, left. Upon introduction of a small interaction with the external magnetic field, the energies of two of the triplet states change, as is clear from the Zeeman term in the spin Hamiltonian. This is shown in figure 1.6b, right, where also the EPR transitions are represented according to the selection rule $\Delta M_s = \pm 1$.

The EPR spectrum corresponds to two transitions that coincide at the average resonance field of the spins 1 and 2. They will no longer coincide if the spins also experience a dipolar interaction.

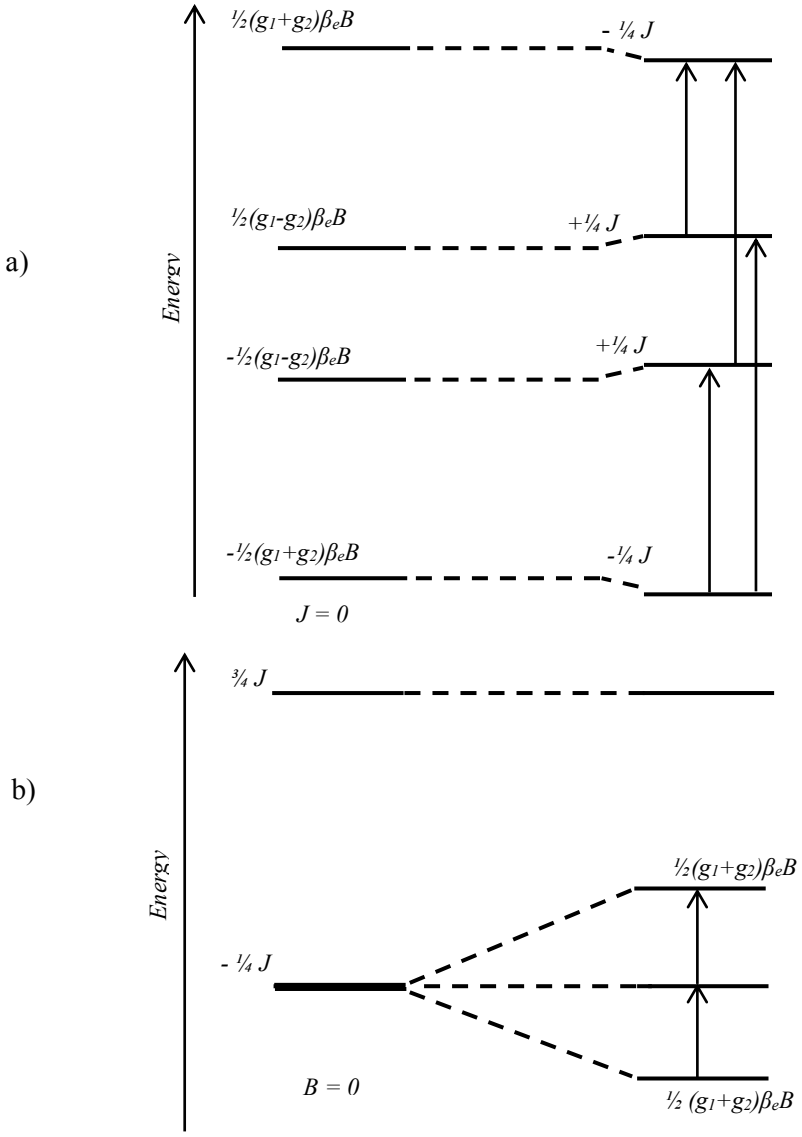

Figure 1.6. Schematic energy-level scheme for a system with the two s=1/2 spins for $J > 0$, neglecting the dipole-dipole interaction for weak coupling, $|J| \ll (|g_1 - g_2|)\beta_e B$ (a), and for strong coupling, $|J| \gg (|g_1 - g_2|)\beta_e B$ (b).

Figure 1.7 shows simulated EPR spectra for a biradical, which illustrate the effect of the magnitude of the exchange interaction. Spectrum (a) at 9.5 GHz exemplifies the weak-coupling case with an exchange coupling of 150 MHz (5.26 mT) of two spins whose g values differ by 0.246, which in frequency units in a field of about 320 mT translates into about 1 GHz. For spectrum (b), again at 9.5 GHz but increasing the exchange coupling to 30 GHz (1.052 T), a single transition is calculated. The strong-coupling limit is reached. With such an exchange coupling, the weak-coupling limit is not reached even in a field of 9 T. The difference in g values of 0.246 in frequency units then amounts to about 30 GHz, i.e., is comparable to the exchange coupling. Spectrum (c) at 275 GHz represents this intermediate case.

For two coupled s=1/2 spins, the EPR spectra strongly depend on the magnetic coupling of the spins as compared to the coupling with the external magnetic field. The latter is an experimental parameter. Changing the microwave frequency of the EPR spectrometer, with the corresponding change of the magnetic field, presents a way to investigate the exchange and dipolar interaction of spins and thereby the electronic structure of a paramagnetic center in a protein. In chapter 4, we will apply this variation of the microwave frequency in the study of the intermediate in the reaction of reduced SLAC with oxygen.

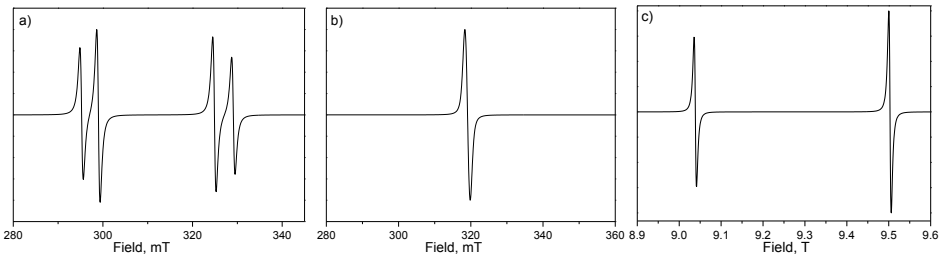

Figure 1.7. Simulated EPR spectra at 40 K of a system of two interacting spins s_1=s_2=1/2 with g_1 = 2.25 and g_2 = 2.004 for J = 150 MHz (a) and J = 30 GHz (b) at 9.5 GHz, and with J = 30 GHz at 275 GHz (c). The spectra are simulated with EasySpin[17] for frozen solutions.

1.6 Thesis outline

The study of the mechanism of the enzymatic reduction of oxygen by SLAC, presents a challenge for EPR spectroscopy. Following the changes in the X-band spectra on the time scale of minutes suggested the presence of a biradical intermediate in the reoxidation of T1D SLAC[12], but EPR studies on the millisecond time scale at multiple microwave frequencies turned out necessary to gain further insight into the nature of the intermediate. We made use of the RFQ/EPR technique, which we improved and extended to enable experiments at microwave frequencies up to 275 GHz.

In chapter 2, we present a modification of the RFQ technique, which improves the collection of the freeze-quench particles from isopentane and their packing into an EPR tube. The method is based on sucking the particle suspension into an EPR tube with a filter at the bottom. This procedure results in a significant reduction of the required volume of reactants, which allows the economical use of valuable reactants such as proteins. The method provides for a reproducible, efficient and fast collection of the freeze-quench particles. We validate the

application of the method to biological samples using the model reaction of binding azide to myoglobin.

In chapter 3, we extend the sucking method described in chapter 2 to small capillaries for higher microwave frequencies. In this way the particles are efficiently packed into the capillaries with inner diameters down to 150 μm, which fit into the single-mode cavities for high-frequency EPR. We demonstrate that one RFQ sample for each point in time suffices for EPR experiments at multiple microwave frequencies, using again the model reaction of binding azide to myoglobin and combining RFQ with EPR at 9, 94 and 275 GHz.

In chapter 4, we make use of RFQ multi-frequency EPR to trap and characterize paramagnetic intermediates formed during the reaction of fully reduced T1D and T1D Y108F SLAC with oxygen on the time scale of milliseconds. For T1D SLAC, a biradical intermediate is detected, which includes tyrosine 108, and could be completely characterized by the combined analysis of EPR data at 9, 94 and 275 GHz. For Y108F T1D SLAC, no biradical intermediate is involved in the reoxidation process. A small contribution of a radical is detected, most probably a tryptophanyl radical.

In chapter 5, we report on the EPR study of the reoxidation of wild-type SLAC under similar experimental conditions as used for the study of T1D SLAC described in chapter 4. The EPR spectra of fully reduced wt SLAC mixed with oxygen on the time scale of milliseconds and longer can be described as the sum of T1 Cu and T2 Cu signals. We find no indications for a biradical or a native intermediate in the single turnover of wild-type SLAC.

In chapter 6, we propose a mechanism for the reaction of O_2 with the reduced T1D SLAC on the basis of our rapid freeze-quench multi-frequency EPR experiments on T1D and T1D Y108F SLAC presented in chapter 4 and

previously obtained optical data on these mutants. We discuss the similarities and differences in the mechanism of O_2 reduction by SLAC, a 2dMCO, with the mechanism proposed for 3dMCO's.

References

(1) Solomon, E. I.; Augustine, A. J.; Yoon, J. O_2 Reduction to H_2O by the Multicopper Oxidases. *Dalton Trans.* **2008**, *9226* (30), 3921–3932.

(2) Yoshikawa, S.; Shimada, A. Reaction Mechanism of Cytochrome c Oxidase. *Chem. Rev.* **2015**, *115* (4), 1936–1989.

(3) Wherland, S.; Farver, O.; Pecht, I. Multicopper Oxidases: Intramolecular Electron Transfer and O_2 Reduction. *J. Biol. Inorg. Chem.* **2014**, *19*, 541–554.

(4) Hellman, Nathan E.; Gitlin, J. D. Ceruloplasmin Metabolism and Function. *Annu. Rev. Nutr.* **2002**, *22*, 439–458.

(5) Singh, S. K.; Grass, G.; Rensing, C.; Montfort, W. R. Cuprous Oxidase Activity of CueO from Escherichia Coli Cuprous Oxidase Activity of CueO from Escherichia Coli. *J. Bacteriol.* **2004**, *186* (22), 7815–7817.

(6) Pardo, I.; Camarero, S. Laccase Engineering by Rational and Evolutionary Design. *Cell. Mol. Life Sci.* **2015**, *72* (5), 897–910.

(7) Giardina, P.; Faraco, V.; Pezzella, C.; Piscitelli, A.; Vanhulle, S.; Sannia, G. Laccases: A Never-Ending Story. *Cell. Mol. Life Sci.* **2010**, *67* (3), 369–385.

(8) Komori, H.; Higuchi, Y.; Ions, F. C. Structural Insights into the O_2 Reduction Mechanism of Multicopper Oxidase. *J. Biochem.* **2015**, *158* (4), 293–298.

(9) Skálová, T.; Dohnálek, J.; Østergaard, L. H.; Østergaard, P. R.; Kolenko, P.; Dušková, J.; Štěpánková, A.; Hašek, J. The Structure of the Small Laccase from Streptomyces Coelicolor Reveals a Link between Laccases and Nitrite Reductases. *J. Mol. Biol.* **2009**, *385* (4), 1165–1178.

(10) Solomon, E. I.; Hadt, R. G. Recent Advances in Understanding Blue Copper Proteins. *Coord. Chem. Rev.* **2011**, *255* (7-8), 774–789.

(11) Machczynski, M. C.; Vijgenboom, E.; Samyn, B.; Canters, G. W. Characterization of SLAC: A Small Laccase from Streptomyces Coelicolor with Unprecedented Activity. *Protein Sci.* **2004**, *13* (9), 2388–2397.

(12) Tepper, A. W. J. W.; Milikisyants, S.; Sottini, S.; Vijgenboom, E.; Groenen, E. J. J.; Canters, G. W. Identification of a Radical Intermediate in the Enzymatic Reduction of Oxygen by a Small Laccase. *J. Am. Chem. Soc.* **2009**, *131* (33), 11680–11682.

(13) Stubbe, J.; Van der Donk, W. A. Protein Radicals in Enzyme Catalysis. *Chem. Rev.* **1998**, *98* (2), 705–762.

(14) Bray, R. C. Sudden Freezing as a Technique for the Study of Rapid Reactions. *Biochem. J.* **1961**, *81*, 189–193.

(15) Tsai, A. L.; Berka, V.; Kulmacz, R. J.; Wu, G.; Palmer, G. An Improved Sample Packing Device for Rapid Freeze-Trap Electron Paramagnetic Resonance Spectroscopy Kinetic Measurements. *Anal. Biochem.* **1998**, *264* (2), 165–171.

(16) Karlin, Kenneth D.; Tyeklár, Z. Bioinorganic Chemistry of Coppers. *Chapman Hall* **1993**.

(17) Stoll, S.; Schweiger, A. EasySpin, a Comprehensive Software Package for Spectral Simulation and Analysis in EPR. *J. Magn. Reson.* **2006**, *178* (1), 42–55.

(18) Hore, P. Dipole-Dipole and Exchange Couping. In *the 5th EF-EPR Summer School on Advanced EPR Spectroscopy*; Konstanz, Germany, **2010**.